# A Temperature-Compensated High-Resolution Microwave Sensor Using Artificial Neural Network

Nazli Kazemi, Mohammad Abdolrazzaghi, *Member, IEEE*, Petr Musilek, *Senior Member, IEEE*, and Mojgan Daneshmand

***Abstract*— In this study, a loss-compensated microwave (MW) planar sensor is used to characterize fluids at ∼1 GHz. The environmental temperature is shown to adversely impact the recorded resonance frequency of the MW sensor, leading to data mixing. This issue is resolved using a feedforward artificial neural network with two hidden layers. Various concentrations of methanol in water (0%–100% with 10% increments) are measured at temperatures ranging between 22 °C and 60 °C. This smart sensor system exhibits a strong ability to discriminate the correct data regardless of erroneous interfering factors up to 92%.**

***Index Terms*— Artificial neural network (ANN), machine learning, microwave (MW) sensor, split-ring resonator (SRR), temperature compensation.**

## I. Introduction

MICROWAVE (MW) sensors have seen profound interest in the past decade; the majority of them incorporate split-ring resonators (SRRs) [1]–[4]. The main drivers to use SRRs as the sensing elements are their compact size, versatile design for fabrication, high sensitivity to capacitive/resistive loading, and, most importantly, the ability of noncontact sensing. Planar SRRs in the MW regime enable noncontact detection and sensing for various applications, including fluidic sensing, gas detection, and biological sample analysis. Despite low maintenance costs and high sensor endurance in noncontact sensors, any unwanted and uncontrolled temperature change in the environment impacts the results [5], [6]. Analog temperature compensation techniques have limited reliability since the values of compensation circuit components also undergo uncertain variations and drift over time. In addition, any hardware compensation is costly and adds to the system complexity. Software compensation offers a feasible alternative.

We propose to use an artificial neural network (ANN) to model the behavior of the MW sensor and to eliminate the uncertainty caused by uncontrolled temperature variations on the sensor response [7], [8]. Recently, ANNs have shown high efficiency and accuracy as learning techniques for complex, nonlinear, and dynamic variations [9]–[11]. Neural models are fast and more accurate than empirical models. They are adaptive by design and fault-tolerant because the failure of a single link does not affect the model performance in a noticeable way.

Temperature variant sensing condition is commonly present in industrial applications. Conventionally, it is considered as an undesired error source from the sensor only, compensating which is presented in the literature with a reference resonator [12], [13]. For this reason, in this study, we have employed a compensation scheme using multilayer perceptron ANN to consider both dielectric constant variation and the active sensory element (transistor). Consequently, the proposed ANN is used to restore sensor response for material under test (MUT) regardless of the environment temperature change. Therefore, this approach is highly effective to resolve the overlap in dielectric constant of materials with varying temperature. The effectiveness of the model is examined in discerning methanol–water solutions.

## II. Problem Statement

Material characterization in the MW regime is practiced using SRRs as sensing elements with a gap sensitive to capacitive changes. An SRR with the length of (($\lambda_g/2$) = 11 cm half-wavelength) is designed according to the defined expressions in [14] to resonate at ∼1 GHz on Rogers 5880 substrate ($\varepsilon_r = 2.2$ and $\tan\delta = 0.0009$). Since various MUTs have different dielectric constants, they impact the sensor differently. Especially, when the MUT has high dielectric loss, the sensor resonant profile degrades which limits the sensor performance. To compensate for the generated loss, a controlled positive feedback [1], [15]–[17] is applied to the sensor as shown in Fig. 1. This loss compensation retrieves the sensor's capability and improves the quality factor. However, the presence of an active device in the sensing platform adds to the temperature drift of the output. The variation of sensor's resonance frequency is measured in an enclosed environment with a heat source that raises the temperature from 22 °C to ∼60 °C (see Fig. 2).

Dielectric constants of materials, that represent their electrical characteristics, are also a function of many other factors such as frequency, temperature, molecular polarizability, etc. This dependence is well-expressed, according to Kirkwood theory for a pure fluid, as follows [18]:

$$\frac{(\varepsilon-1)(2\varepsilon+1)}{9\varepsilon} = \frac{4\pi\rho N_{\mathrm{A}}}{3M}\left(\alpha + \frac{\mu^2 g}{3k_{\mathrm{B}}T}\right) \quad (1)$$

Manuscript received June 14, 2020; revised July 9, 2020; accepted July 17, 2020. This work was supported in part by the Canadian Research Chair Program, in part by the National Science and Engineering Research Council of Canada, and in part by CMC Microsystems. *(Corresponding authors: Nazli Kazemi; Mohammad Abdolrazzaghi.)*

Nazli Kazemi, Mohammad Abdolrazzaghi, and Petr Musilek are with the Department of Electrical and Computer Engineering, University of Alberta, Edmonton, AB T6G 1H9, Canada (e-mail: nazli@ualberta.ca; mabdolra@ualberta.ca; petr.musilek@ualberta.ca).

Mojgan Daneshmand, deceased, was with the Department of Electrical and Computer Engineering, University of Alberta, Edmonton, AB T6G 1H9, Canada.

Mojgan Daneshmand was one of the victims of the Ukrainian plane crash on January 8, 2020. This letter is dedicated to her memory.

Color versions of one or more of the figures in this letter are available online at http://ieeexplore.ieee.org.

Digital Object Identifier 10.1109/LMWC.2020.3012388

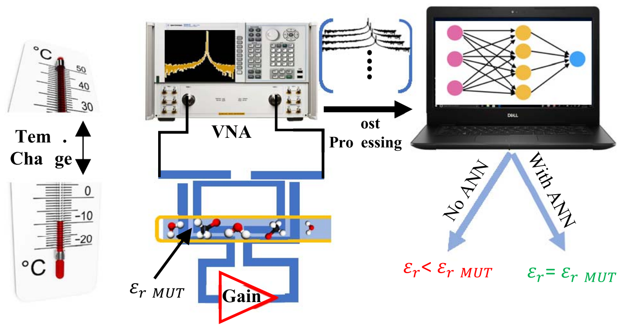


Fig. 1. Temperature impact on MUT sensing.

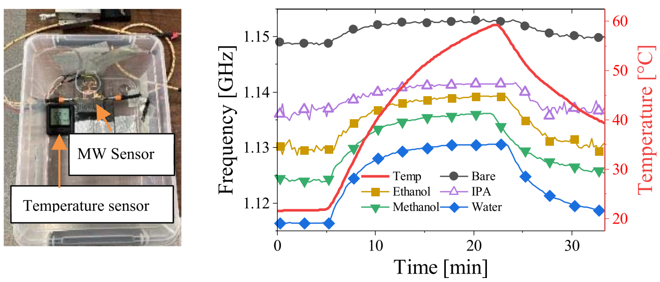


(a) (b)

Fig. 2. (a) Sensing setup in controlled temperature varying environment. (b) Sensor response with/without MUT to temperature rise and fall.

where $M$ is molecular weight, $\rho$ is density, $\alpha$ is molecular polarizability, $N_A$ is Avogadro's number, $\mu$ is dipole moment of the molecule, $k_B$ is Boltzmann's constant, and $g$ is a correlation factor that characterizes the relative orientation between neighboring molecules.

This expression explains the inverse and nonlinear relationship between temperature and the dielectric constant of fluids. As an example of the permittivity variation, 10 °C increase in temperature (from 283.15 to 293.15 K) reduces the permittivity of common liquids as shown in Table I.

The sensor confirms this dependence with an upshift of the resonance frequency, as shown in Fig. 2(b) for water, methanol, isopropyl alcohol (IPA), and ethanol. Considering the variation of the bare resonator to temperature is ~5 MHz from $T_1 = 22$ °C to $T_2 = 60$ °C (see Fig. 2), the sensor with MUT responds to temperature much more [see Fig. 2(b)]. It can be inferred that the temperature increase reduces the density of MUT, and thus the frequency shifts up. This shift is more significant for higher permittivity materials. This analysis highlights the significance of errors that can occur in characterizing fluids based on a conventional method of tracking the resonance frequency.

## III. Proposed Solution

To avoid the errors in characterizing fluids, we propose to develop and train an ANN to discriminate the MUTs regardless of temperature variation. The structure of the network and the training data are shown in Fig. 3(a).

For each MUT, the values of forwarding transmission $|S_{21}|$ are recorded at specific time intervals as the temperature varies, and then used as one row of the training data set. Each row is then augmented with a value representing the material type. Each color in the data set signifies the sensor response for one type of material at different temperatures. This forms a bundle of $|S_{21}|$ values that belong to a single MUT. Other similar bundles of $|S_{21}|$ are created for other existing MUTs covering the temperature range of interest. A stack of all bundles constitutes the full data set, as presented in Fig. 3(a). ANN trained with this data will map all $|S_{21}|$ profiles into the correct material type, as the characterization data set inherently, includes the temperature effect. It is expected that after training, the algorithm can correlate any measured $S_{21}$ to its closest response and identify the material type regardless of the temperature.

TABLE I
Dielectric Constant of Selected Materials Calculated by the Kirkwood Model

| Component | Calculated $\varepsilon$ | |
|---|---|---|
| | 283.15 K | 293.15 K |
| **Water** | 83.92 | 80.1 |
| **Methanol** | 36.96 | 33.1 |
| **Ethanol** | 26.58 | 25.1 |
| **Acetone** | 22.72 | 21.4 |

It should be noted that since the frequency of resonance does not provide information sufficient for MUT discrimination, more information on the resonance profile is required. Therefore, the entire transmission profile ($|S_{21}|$, magnitude only) is used to cover all principal features of resonance, including resonance frequency, amplitude, and quality factor.

Each column in the data set of Fig. 3(a) is assigned to a neuron in the input layer of the ANN. The input neurons only distribute (fan-out) the incoming values to the neurons of the first hidden layer. All remaining neurons of the network process their incoming signals as follows:

$$y_j = f\left(\sum_i w_{ij} x_i + b_j\right) \tag{2}$$

where $x_i$ and $y_j$ are neuron inputs and output, respectively, $w_{ij}$ are weights, $b_j$ is a bias term, and $f$ is a nonlinear activation function. The goal of the training is to update the weights to minimize the loss (approximation error). The error is determined by comparing the actual output of the network with the desired output (the MUT label obtained from the training data set). While the size of the input and output layer is given by the problem at hand, the number of hidden layers and neurons is a design choice that needs to be validated or optimized [19].

## IV. Results and Discussion

To verify the functionality of the proposed algorithm, different concentrations of methanol in water were prepared from 0% to 100%, with 10% increments (11 samples in total). This choice of fluids allows analyzing a wide range of permittivity values from $\varepsilon_{r_{\text{methanol}}} = 30$ to $\varepsilon_{r_{\text{water}}} = 80$ [20], [21], as shown in Fig. 3(b). A predefined heating process is applied to all MUTs with 20 initial recordings at the room temperature (~22 °C). During the heating process, the chamber's temperature increases up to ~60 °C in ~25 min. A commercial temperature sensor with an accuracy of 0.5 °C also records the chamber's temperature. This all translates to 150 data points (recorded transmission profiles) per concentration. The recorded profiles are limited to the span shown in Fig. 3(c), which captures the first ($T = 22$ °C) and the last ($T = 60$ °C) profile of water and methanol. The resultant mixtures (concentrations of 10%–90% methanol-in-water) have transmission profiles between these two extremes. The frequency span used

This article has been accepted for inclusion in a future issue of this journal. Content is final as presented, with the exception of pagination.



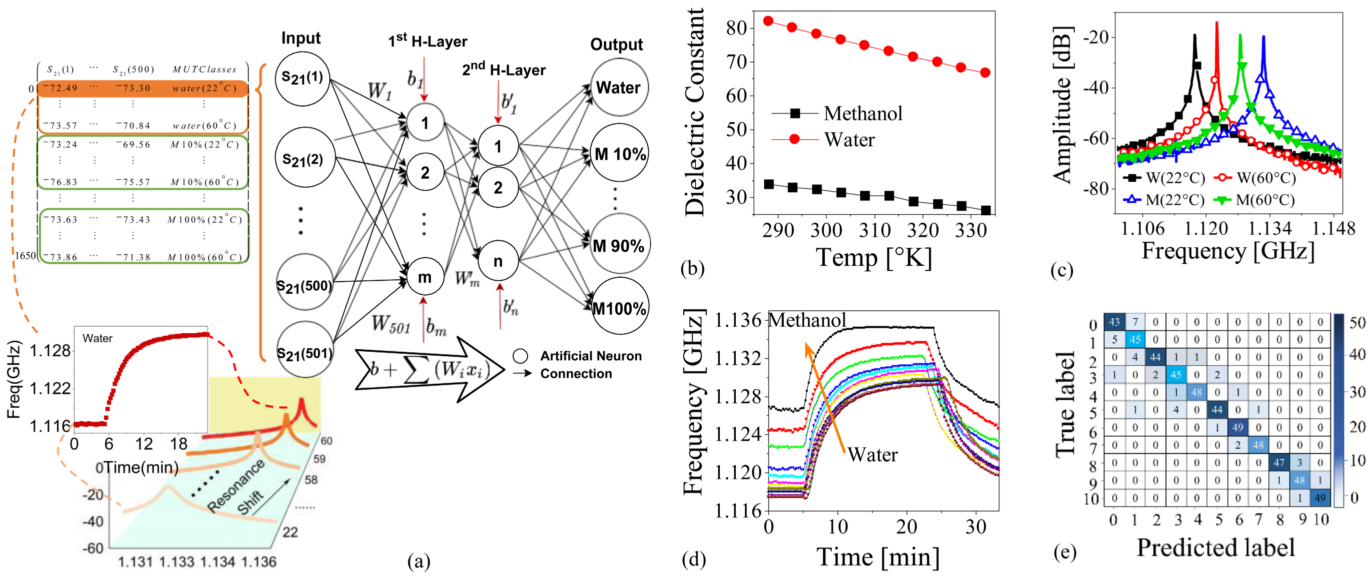

Fig. 3. (a) ANN diagram for MUT discrimination. (b) Dielectric constant variation of water and methanol between low- and high-end temperature. (c) Transmission profile of the sensor for methanol and water exposed to temperature ramp of 22 °C–60 °C. (d) Frequency shifts for various concentrations of methanol in water with increment of 10%. (e) Confusion matrix from ANN.

in this analysis [1.1–1.15 GHz, as shown in Fig. 3(c)] contains 500 points in each $|S_{21}|$ Profile.

The recorded transmission profiles (500 columns for $|S_{21}|$ with another last column for material type) comprise 150 rows for each material. This is one building block in a large data set of 1650 by 501 values, shown in Fig. 3(a), after combining 11 material types (classes) vertically. Two-thirds (100) of input rows for each class are randomly selected to train the ANN, and the remaining one-third is used as the test set. The ANN consists of two hidden layers, with 100 and 40 neurons, respectively. Once the training is completed, the test set is used to verify whether the ANN maps each input to its corresponding class.

The performance of the algorithm can be visualized using confusion matrix. It shows how well the classifier performs, with respect to the individual material types. The confusion matrix is populated based on the test set whose true outputs (labels) are known. Each row of this matrix [see Fig. 3(d)] represents how the data within a known class is mapped to the correct class. For example, row 4 explains 48 out of 50 test cases are correctly predicted, while two are mistakenly predicted as class 3 and 6. The color spectrum shows how well each input test set is predicted: light color means low accuracy and vice versa. Fully correct mapping can be distinguished with zeros at all elements except the one at the diagonal. In a close look at the confusion matrix, it is clear that the lower concentrations (<30%) show lower accuracy. This can be explained with respect to Fig. 3(c) that showcases the resonance frequencies of the transmission profiles, where, regardless of temperature, sensor frequency response saturates as dielectric constant increases. This phenomenon causes high cross correlation in the resonance frequency curves of materials with higher values of dielectric constant. Thus, the network has a poor performance for higher dielectric constants (lower concentrations). The parameters of the network, including number of layers/neurons, optimizers, etc., should be optimized to resolve this issue. The total accuracy for all test data of all classes is 92%, a considerably high value given the elimination of temperature impact on sensing.

TABLE II
COMPARISON TABLE BETWEEN MW PLANAR SENSORS

| Ref | Sensing Element | $f_0[GHz]$ | Q | Temp. compensation |
|---|---|---|---|---|
| [22] | OCSRRs | 1.125 | 2* | No |
| [23] | Omega Resonator | 1.9 | 8* | No |
| [24] | OSRR | 6.5 | 72* | No |
| [12] | OSRR | 2.5 | 327 | Yes |
| [25] | CSRR | 2.4 | 36* | No |
| **This Work** | SRR | 1 | 3700 | Yes |

*: approximated from figures

A comparison between this study and prevalent MW sensors is given in Table II. The proposed sensor is highly potent for use in harsh environments, including lossy material sensing. The quality factor of the sensor, which is prominent in characterizing lossy medium, is restored to $Q \sim 3700$, an order of magnitude higher than the recent planar sensors to evade a flatten profile using the positive feedback circuit. Moreover, the erroneous temperature effect is omitted from both the sensor and MUT using ANN with a single resonator, as opposed to [12], wherein temperature impact is removed from only the sensor, not MUT, with two resonators.

## V. CONCLUSION

A loss-compensated MW planar sensor is used for material characterization, yet, environmental temperature is varied as an extraneous parameter. The resonance profile of the system is shown to drift due to the circuit and also changes in the dielectric constant of the fluids. This erroneous variation in sensory systems is removed with proper incorporation of ANN with two hidden layers. Various concentrations of methanol in water were classified with high accuracy of 92% on testing data. This enables MW sensors to be employed in variant environments when equipped with the adaptive ANN system.

## REFERENCES


[1] M. Abdolrazzaghi and M. Daneshmand, "A phase-noise reduced microwave oscillator sensor with enhanced limit of detection using active filter," *IEEE Microw. Wireless Compon. Lett.*, vol. 28, no. 9, pp. 837–839, Sep. 2018.

[2] M. Abdolrazzaghi, M. H. Zarifi, and M. Daneshmand, "Wireless communication in feedback-assisted active sensors," *IEEE Sensors J.*, vol. 16, no. 22, pp. 8151–8157, Nov. 2016.

[3] S. Mohammadi, A. V. Nadaraja, K. Luckasavitch, M. C. Jain, D. June Roberts, and M. H. Zarifi, "A label-free, non-intrusive, and rapid monitoring of bacterial growth on solid medium using microwave biosensor," *IEEE Trans. Biomed. Circuits Syst.*, vol. 14, no. 1, pp. 2–11, Feb. 2020.

[4] A. Ebrahimi, J. Scott, and K. Ghorbani, "Ultrahigh-sensitivity microwave sensor for microfluidic complex permittivity measurement," *IEEE Trans. Microw. Theory Techn.*, vol. 67, no. 10, pp. 4269–4277, Oct. 2019.

[5] H. Wang, W. Zhang, L. You, G. Yuan, Y. Zhao, and Z. Jiang, "Back propagation neural network model for temperature and humidity compensation of a non dispersive infrared methane sensor," *Instrum. Sci. Technol.*, vol. 41, no. 6, pp. 608–618, Nov. 2013.

[6] Z. Nenova and G. Dimchev, "Compensation of the impact of disturbing factors on gas sensor characteristics," *Acta Polytech. Hungarica*, vol. 10, no. 3, pp. 97–111, 2013.

[7] M. Abdolrazzaghi, M. H. Zarifi, W. Pedrycz, and M. Daneshmand, "Robust ultra-high resolution microwave planar sensor using fuzzy neural network approach," *IEEE Sensors J.*, vol. 17, no. 2, pp. 323–332, Jan. 2017.

[8] M. Abdolrazzaghi, S. Hashemy, and A. Abdolali, "Fast-forward solver for inhomogeneous media using machine learning methods: Artificial neural network, support vector machine and fuzzy logic," *Neural Comput. Appl.*, vol. 29, no. 12, pp. 1583–1591, Jun. 2018.

[9] J. Rivera, M. Carrillo, M. Chacón, G. Herrera, and G. Bojorquez, "Self-calibration and optimal response in intelligent sensors design based on artificial neural networks," *Sensors*, vol. 7, no. 8, pp. 1509–1529, Aug. 2007.

[10] A. P. Singh, T. S. Kamal, and S. Kumar, "Development of ANN-based virtual fault detector for wheatstone bridge-oriented transducers," *IEEE Sensors J.*, vol. 5, no. 5, pp. 1043–1049, Oct. 2005.

[11] H. Rahmani *et al.*, "Towards a machine-learning-assisted dielectric sensing platform for point-of-care wound monitoring," *IEEE Sensors Lett.*, vol. 4, no. 6, pp. 1–4, Jun. 2020.

[12] A. A. Abduljabar, H. Hamzah, and A. Porch, "Double microstrip microfluidic sensor for temperature correction of liquid characterization," *IEEE Microw. Wireless Compon. Lett.*, vol. 28, no. 8, pp. 735–737, Aug. 2018.

[13] A. A. Abduljabar, N. Clark, J. Lees, and A. Porch, "Dual mode microwave microfluidic sensor for temperature variant liquid characterization," *IEEE Trans. Microw. Theory Techn.*, vol. 65, no. 7, pp. 2572–2582, Jul. 2017.

[14] M. Abdolrazzaghi, M. H. Zarifi, C. F. A. Floquet, and M. Daneshmand, "Contactless asphaltene detection using an active planar microwave resonator sensor," *Energy Fuels*, vol. 31, no. 8, pp. 8784–8791, Aug. 2017.

[15] M. H. Zarifi, M. Fayaz, J. Goldthorp, M. Abdolrazzaghi, Z. Hashisho, and M. Daneshmand, "Microbead-assisted high resolution microwave planar ring resonator for organic-vapor sensing," *Appl. Phys. Lett.*, vol. 106, no. 6, Feb. 2015, Art. no. 062903.

[16] Z. Abbasi, H. Niazi, M. Abdolrazzaghi, W. Chen, and M. Daneshmand, "Monitoring pH level using high-resolution microwave sensor for mitigation of stress corrosion cracking in steel pipelines," *IEEE Sensors J.*, vol. 20, no. 13, pp. 7033–7043, Jul. 2020.

[17] Z. Abbasi, P. Shariaty, M. Nosrati, Z. Hashisho, and M. Daneshmand, "Dual-band microwave circuits for selective binary gas sensing system," *IEEE Trans. Microw. Theory Techn.*, vol. 67, no. 10, pp. 4206–4219, Oct. 2019.

[18] P. Wang and A. Anderko, "Computation of dielectric constants of solvent mixtures and electrolyte solutions," *Fluid Phase Equilibria*, vol. 186, nos. 1–2, pp. 103–122, Aug. 2001.

[19] H. B. Demuth, M. H. Beale, M. T. Hagan, and O. D. Jess, *Neural Network Design*, 2nd ed. Boston, MA, USA: PWS Publishing Co., 2014.

[20] N. Deb and A. K. Mukherjee, "Dielectric constant of water from free energies of H-bond formation in $(H_2O)_n$ clusters," *Chem. Phys. Lett.*, vol. 462, nos. 4–6, pp. 243–245, Sep. 2008.

[21] N. Deb, A. S. Tiwary, and A. K. Mukherjee, "Calculation of the Kirkwood–Frohlich correlation factor and dielectric constant of methanol using a statistical model and density functional theory," *Mol. Phys.*, vol. 108, no. 14, pp. 1907–1917, Jul. 2010.

[22] P. Velez, K. Grenier, J. Mata-Contreras, D. Dubuc, and F. Martin, "Highly-sensitive microwave sensors based on open complementary split ring resonators (OCSRRs) for dielectric characterization and solute concentration measurement in liquids," *IEEE Access*, vol. 6, pp. 48324–48338, 2018.

[23] Y. I. Abdulkarim *et al.*, "Novel metamaterials-based hypersensitized liquid sensor integrating omega-shaped resonator with microstrip transmission line," *Sensors*, vol. 20, no. 3, p. 943, Feb. 2020.

[24] J. A. Byford, K. Y. Park, and P. Chahal, "Metamaterial inspired periodic structure used for microfluidic sensing," in *Proc. IEEE 65th Electron. Compon. Technol. Conf. (ECTC)*, May 2015, pp. 1997–2002.

[25] X. Zhang, C. Ruan, T. Haq, and K. Chen, "High-sensitivity microwave sensor for liquid characterization using a complementary circular spiral resonator," *Sensors*, vol. 19, no. 4, p. 787, Feb. 2019.